Bulletin of the Seismological Society of America, Vol. 99, No. 2A, pp. 761–773, April 2009, doi: 10.1785/0120080179

V_{S30} Estimates Using Constrained H/V Measurements

by Silvia Castellaro and Francesco Mulargia

Abstract Most seismic codes adopt the average shear-wave velocity as a key parameter in the first 30 m of subsoil (V_{S30}). Estimates of V_{S30} are therefore required for both large- and small-scale seismic microzonation. We propose a technique to measure the V_{S30} based on the horizontal to vertical spectral ratio (H/V) of microtremor recorded at a single station. The H/V is fitted with a synthetic curve using the independently known thickness of a superficial layer of the subsoil as a constraint. The proposed procedure consists of three steps: (1) identify the depth of a shallow stratigraphic horizon from independent geotechnical data, (2) identify its corresponding H/V marker, and (3) use it as a constraint to fit the experimental H/V curve with the theoretical one. The synthetic H/V curve is calculated by assuming a stratified one-dimensional (1D) soil model and a tremor wave field from distant random sources that are composed of Rayleigh and Love waves. This technique has been validated on different geological settings following a triple check procedure: (1) the theoretical Rayleigh-wave phase velocity dispersion curves calculated for the model derived from the H/V fit were compared to the experimental curves measured with the 2D extended spatial autocorrelation (ESAC) method and the 1D refraction microtremor (ReMi) array surveys; (2) the V_S profiles and (3) the V_{S30} estimates obtained by the proposed technique were compared to those obtained by using the latter array techniques. Finally, the inferred stratigraphy was compared to the geological model. The proposed technique is not meant to provide accurate V_S profiles but has the potential to provide V_{S30} estimates that are coherent with those measured through ESAC and ReMi and to satisfy law requirements. Furthermore, the H/V is found to be capable in detecting deviations from 1D subsoil geometry over the length of a few meters, the correctness of which was confirmed by direct drilling.

Introduction

Traditionally, the geophysical approach to seismic risk has given the highest priority to the estimate of seismic hazard, that is, the probability that an earthquake of a given magnitude may occur in a given area within a given period of time. However, another factor was recently found to be important, that is, the mapping of site amplification effects. An attempt to combine these two elements has been recently presented by Parolai *et al.* (2007).

There is no full consensus on the most effective procedure for estimating the potential site amplification effects beforehand. The most common parameter adopted worldwide is the average shear-wave velocity in the first 30 m of subsoil (V_{S30}), which is used to classify soils into a small number of classes (5–7), although any statistical test would conclude that this parameter has no (or a very weak) link to seismic amplification (Castellaro *et al.*, 2008).

A large number of active and passive geophysical techniques is already available to measure the V_S profile; however, the fact that the estimate of V_{S30} is required at not only large scale for regional microzonation, but also at the scale of the single building for designing its foundations, creates a number of practical problems. These are related to the fact that the measure of the *S*-wave velocity profile using seismic methods requires specific apparatuses and, according to some active methods, extensive drilling. The goal of the present article is to propose a fast and inexpensive technique to estimate the V_{S30} based on the horizontal to vertical spectral ratio (H/V) of microtremor recorded at a single station. The proposed approach appears to be adequate in satisfying the existing building codes.

Proposed Technique

There is a general consensus on the fact that, in a single layer one-dimensional (1D) stratigraphy, the analysis of the H/V of the microtremor allows us to measure the principal *S*-wave resonance frequency f of the sedimentary cover overlying an infinite bedrock with reasonable accuracy. This is linked to the thickness h and the average *S*-wave velocity (V_S) of the sedimentary layer (Lermo and Chavez-Garcia,

1993, 1994; Lachet and Bard, 1994; Ibs-von Seht and Wohlenberg, 1999; Fäh *et al.*, 2001) by

$$f = \frac{V_S}{4h}. \quad (1)$$

One could attempt to refine equation (1) by accounting for the gravitational compaction of sediments in order to extend its validity to greater depths than a few meters (Ibs-Von Seht and Wohlenberg, 1999). However, the existence of a single layer of sediments is almost never encountered in practice over substantial depths. In general, there are several alternated layers of different lithology; these can produce an H/V curve with several peaks and troughs. Assuming an appropriate model for the wave field and the medium, a theoretical H/V curve can be fitted to the experimental one to infer a subsoil model, provided that the inversion is sufficiently constrained. We propose using the thickness of the most superficial layer, which is independently known in most cases from geotechnical practice, as a constraint.

Procedure

Without any constraint, an H/V curve can be fitted by an infinite number of synthetic models. The proposed procedure requires information about the shallow subsoil stratigraphy (alternatively, the V_S of the first layer—when available from independent methods—can be used). In particular, it is necessary to know the depth of a discontinuity (h_1), which is, in geotechnical practice, generally provided from penetration tests, drillings, pits, and trenches. The stratigraphy does not need to be known down to 30 m.

The proposed procedure consists of the following steps:

1. Measure the H/V. This requires 15–20 min of recording with appropriate instruments and can be effected everywhere (no need for cable deployment, diggings, etc.).
2. Identify the H/V marker corresponding to the known superficial stratigraphic horizon with a depth h_1.
3. Use h_1 to constrain the fit of the synthetic H/V curve to the measured one.
4. Fit a synthetic H/V curve to the experimental one.

The H/V analyses that are presented in this study were performed as described in Castellaro *et al.* (2005). We used 20 sec windows to obtain the average H/V and its 2σ intervals. Attention was paid to the removal of transients from the H/V curve. Panel (a) in Figure 1 shows an average H/V and its 2σ intervals before any cleaning procedure. It is clear that below 2 Hz, the H/V curve suffers from a few noisy windows that can be easily identified and removed in panel (b), where the H/V time stability is shown. Each vertical bar in this

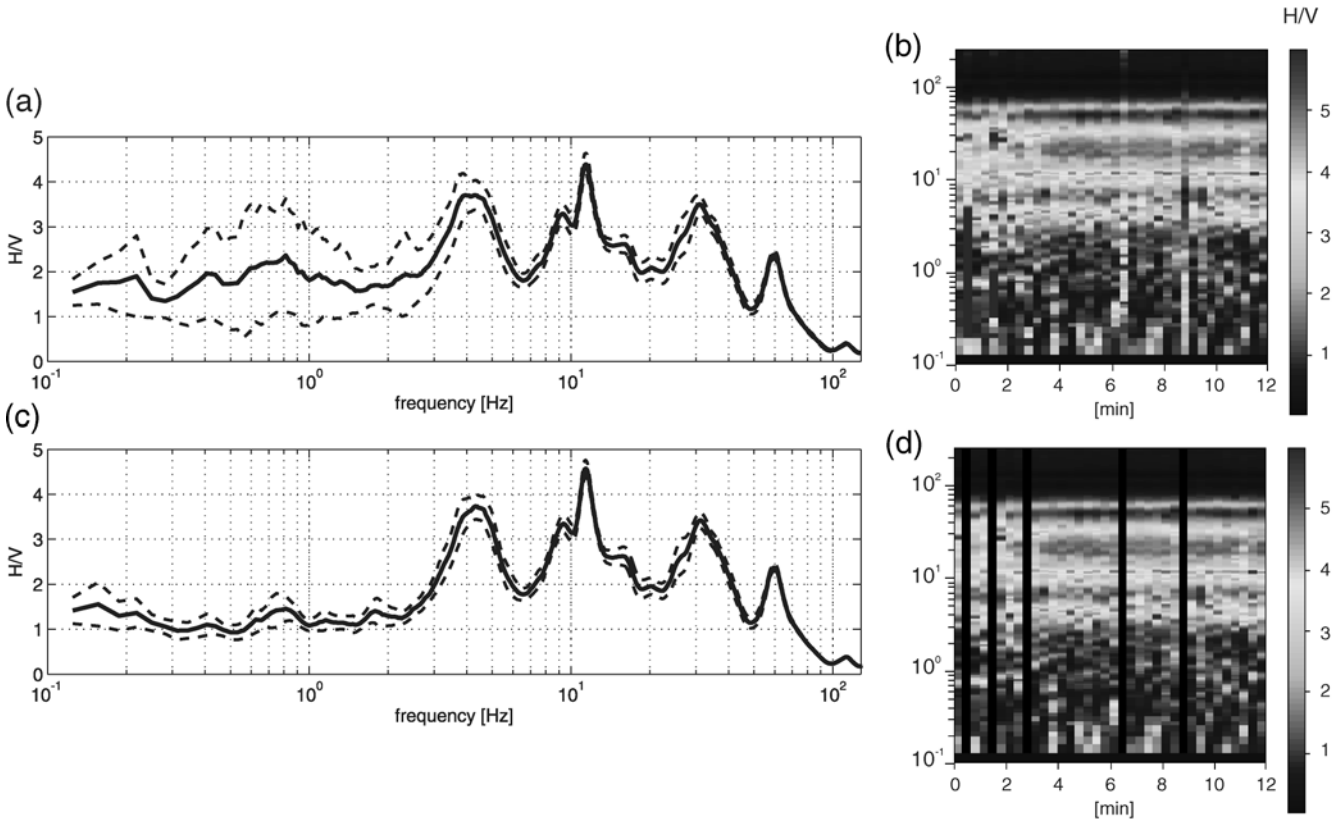

Figure 1. Average H/V (solid lines) and 2σ intervals (dashed lines) recorded at the same site before (a) and after (c) the removal of noisy transients. (b) Time stability of the H/V curve during the measurements (H/V amplitude in gray scale; time on the *x* axis; frequency on the *y* axis). (d) Time windows remaining after the transient removal.

panel illustrates (H/V amplitude in color versus frequency on the *y* axis) the H/V time history (*x* axis). The removal of a few time windows in which the signal deviates from the average (panel [d]) produces a much cleaner H/V curve (panel [c]), showing that H/V is very stable using 20 sec partitions. This procedure is essential to not interpret statistically insignificant H/V peaks.

The H/V Peak of the Shallow Stratigraphic Horizon

It may be argued that sometimes, at relatively high frequency, no H/V peak associated to a shallow stratigraphic horizon can be observed; thus, the basic requirement for the proposed procedure may not be satisfied. This argument comes from the fact that in the seismic microzonation practice, attention has generally only been paid to the main resonance frequency, which is the largest H/V peak, while other stable humps and troughs in the curve were not considered. Exceptions are found, for example, in the works of Guéguen *et al.* (1998), Bodin *et al.* (2001), and Guillier *et al.* (2005).

It is important to note that recordings taken on homogeneous rock without any cover/weathered layer give flat H/V curves so that the procedure proposed in the present work cannot estimate the V_S profile. However, these cases are of minor interest because no site amplification is expected.

In the other cases, using appropriate instruments and recording protocol, an H/V peak that can be traced back to a shallow stratigraphic discontinuity can generally be observed. However, the operator should be aware of a further feature, that is, the H/V marker of inversions in the V_S profile. This feature has been extensively discussed through theoretical models and experimental examples in Castellaro and Mulargia (2008). Here we simply recall that a natural (e.g., gravel over soft clays) or an artificial (e.g., stiff artificial pavement over soft sediments) inversion in the V_S profile is persistently signaled by an H/V ratio below 1, due to the depression of the spectral horizontal components below the vertical one. A velocity inversion can affect the H/V curve amplitude down to 2 Hz. On an $H/V < 1$ curve, there is no peak satisfying the SESAME (2005) empirical rule of thumb ($H/V > 2$) that can be observed at mid- to high frequency. However, because the vertical spectral component remains almost unaffected in shape, an interpretation can still be possible based on the local minimum of the vertical spectral component that gives a bump in the H/V curve, though again with amplitude forcedly below 1. Some practical cases will be discussed later in this work (see the Results section, Sites III and IV, for artificial velocity inversions, and Site V for natural velocity inversion).

As a general rule, because velocity inversions in the V_S profile make the H/V curves more difficult to interpret, the artificial ones often induced by stiff artificial soils (pavements, asphalts, and similar) on softer sediments must be avoided in directly recording microtremor on natural soil.

Fitting the Synthetic H/V Curve

In light of the coherence emerging from array measurements (see SESAME, 2005, and references therein), the usual assumption is that the wave field is composed of surface waves. There are minor doubts on surface wave predominance in tremor but the relative importance of Rayleigh and Love waves still appears to be open to question. The observation of Love waves in tremor has been often claimed (e.g., SESAME, 2005) with widely variable relative weight: for example, Köhler *et al.* (2007) suggest 90% Love waves and 10% Rayleigh waves, while Bonnefoy-Claudet *et al.* (2008) suggest at least 50% Love waves. At the same time, theoretical arguments suggest that Love waves should play a minor role with respect to Rayleigh waves (Campillo and Paul, 2003; Roux *et al.*, 2004; Shapiro and Campillo, 2004) because they are not sufficiently excited from the scatterers in the crust. The contribution of Love waves typically reflects on the H/V amplitude, as illustrated in Figure 2, where the same synthetic models (subsoil model of Site I, Fig. 5) with Rayleigh waves alone or with 50% Rayleigh and 50% Love waves are compared. In this article, we assume a wave field composed of 50% Rayleigh and 50% Love waves.

The experimental evidence of low quality factors Q of subsoils, with values ranging from 1 to a few tens (Malin *et al.*, 1988; Del Pezzo *et al.*, 1991; Malagnini 1996; Jeng *et al.*, 1999; Müller and Shapiro, 2001) stands for a strong wave absorption both by dissipation and scattering. The effect is that low modes are likely to prevail except in the near field of the tremor source. However, in our analyses, we did not explicitly consider the effect of Q.

We restricted our H/V models to the fundamental mode only because the lowest surface wave modes generally carry more energy than the sum of all higher modes in the seismic noise wave field at a single point (Sax and Hartenberg, 1964; Tanimoto, 1987; Romanowicz, 2003). Moreover, in no case among those analyzed did we have evidence of higher modes in the H/V curves. A very different picture is found for arrays, which are sensitive to the coherence of the wave field at different points, which can only be statistically defined (Mulargia and Castellaro, 2008). This will be discussed in the next section.

For the medium, we assumed a 1D stratigraphy and adopted the 1D coupling coefficients of Ben-Menahem and Singh (1981). A Dunkin stability correction (Dunkin, 1965) was used in the propagators.

Validation

We compared the results of our procedure with those of (1) a well-established array technique to infer V_S, that is, the extended spatial autocorrelation (ESAC), as defined by Ohori (2002) and (2) an array technique very popular in the geotechnical practice, that is, the refraction microtremor (ReMi), as defined by Louie (2001). We used 2D arrays for the ESAC analysis and the linear legs of the same arrays for the ReMi analyses.

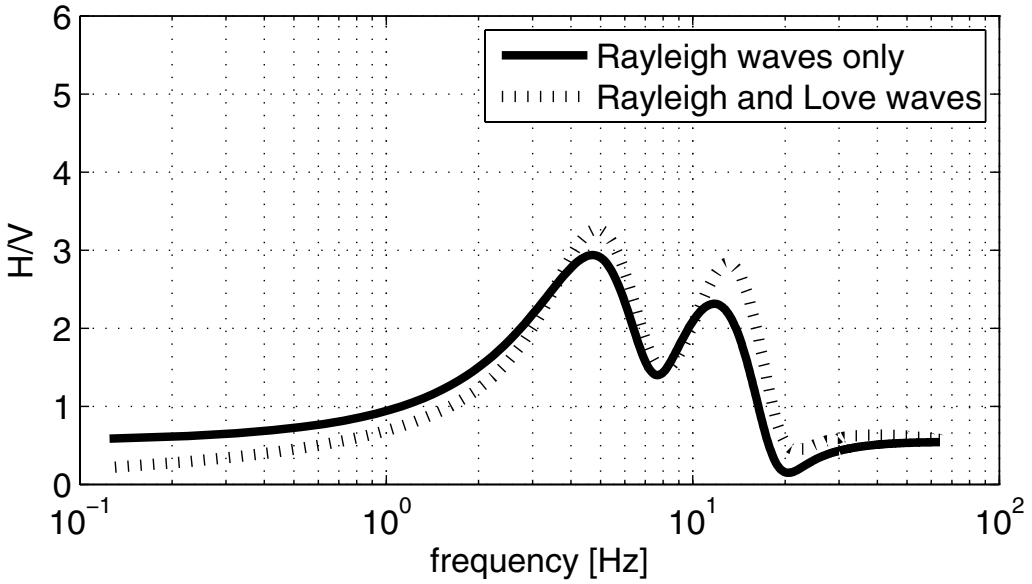

Figure 2. Comparison between a synthetic H/V model produced using Rayleigh waves only (solid line) and using 50% Rayleigh and 50% Love waves (dashed line). The subsoil model is illustrated in Figure 5e.

Seismic arrays are antennas which, according to their specific geometry, are tuned to a fixed set of frequencies and source azimuth. The seismic noise wave field has been shown to have a near-diffuse character, with different apparent sources uniformly distributed over a finite azimuthal aperture and acting at different times (Mulargia and Castellaro, 2008). This statistical definition of sources produces wave trains with fluctuating composition and azimuth which, on a fixed array, result in an unstable picture in time. This is clear in Figure 3, where the frequency-velocity analysis of four consecutive 10 sec windows recorded by the same array at the same site gives four completely different images. Panel (a) shows a dispersion curve where the fundamental mode is clearly visible, panel (b) shows a dispersion curve where only a higher mode (or the dispersion curve of a wave train not aligned with the array) is visible, panel (c) shows a dispersion curve where several fragments of several modes (or the dispersion curve of wave trains not aligned with the array) are visible, and panel (d) does not show any clear dispersion curve. Quite obviously, if noise were recorded only at the time of panel (b), the dispersion curve inverted for the fundamental Rayleigh mode would give a V_S profile a factor of 2 larger than real.

In practice, tremor must be recorded for several minutes and at least some tens of dispersion curves must be calculated on different time windows in order to understand the modal pattern of the dispersion curve. Dispersion curves may vary so largely in time that blind averaging may result in an inconsistent variety of pictures depending on the details of the averages. For example, it may happen that higher modes of unknown order are dominant and the fundamental mode is difficult to identify, making a correct interpretation very hard to achieve.

In our case, we sampled ambient noise continuously for 20 min. Because we aimed at inverting the dispersion curve of the fundamental mode, the dispersion curves were averaged over 10–15 sec time windows, excluding those that did not show a clear dispersion or in which higher modes were dominant.

Active array techniques are affected to an even greater extent by this phenomenon, not due to source fluctuations but to the fact that active sources (hammer, explosion, etc.) have a strong high-frequency content, which excites the higher modes.

We have kept the arrays as short as possible in order to avoid lateral subsoil heterogeneities. In a single case, the array length used in this study was 90 m, while in the majority of cases, arrays were only 35 m long. In spite of this (see the following section), we had evidence of deviations from 1D geometry in many cases.

The validity check of our procedure with the array results was threefold and compared (1) the theoretical Rayleigh-wave phase velocity dispersion curves calculated for the models derived from the H/V fits with the experimental dispersion curves from array measurements, (2) the V_S profile estimates obtained with the proposed technique with those obtained at the same sites by using the latter array techniques, and (3) the V_{S30} estimates from the H/V fits with those obtained at the same sites by using established array techniques. Finally, the inferred stratigraphy was also compared with surface geology and drilling information for geological coherence.

Inversion

From the analysis of the ESAC and ReMi results, we pick a single dispersion curve at each site and invert it

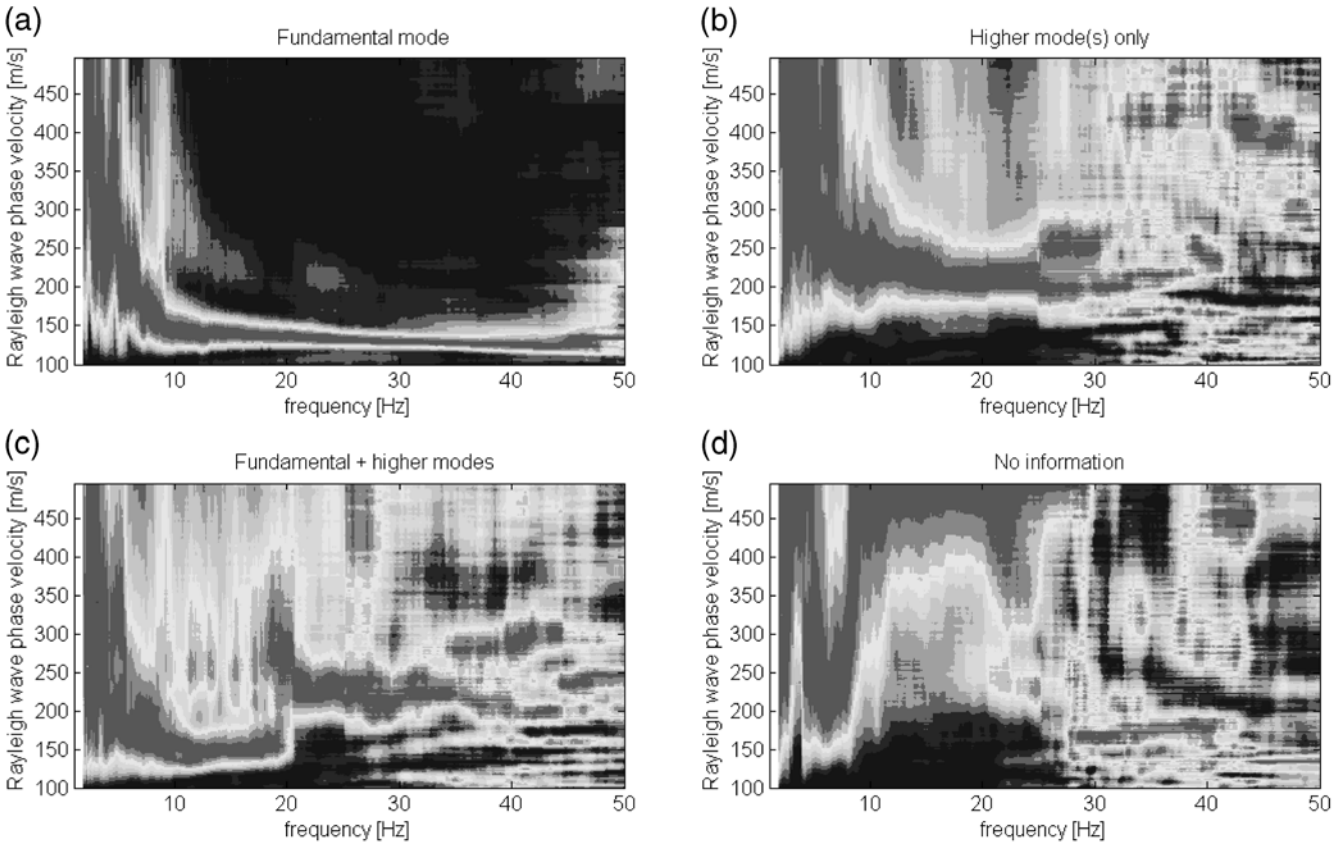

Figure 3. Example of dispersion curves obtained exactly at the same site, by the same array, at different times. Therefore, only the different signal sources may be responsible for the different observed dispersion curves. Each image is produced using 10 sec time windows. (a) Fundamental mode only. (b) Higher mode(s) (or dispersion curves of wave trains not aligned with the array) only. (c) Fundamental + higher mode(s) (or dispersion curves of wave trains not aligned with the array). (d) No clear dispersion curve.

through the Levenberg–Marquardt method (Marquardt, 1963). Six layers and a fixed Poisson ratio for each layer are selected, and the parameter space explored by the algorithm is illustrated in the relative figures. The fit of the H/V curve generally relies on a lower number of layers: a maximum of four for the cases with no velocity inversions and a maximum of six for those with velocity inversions.

Differences from Other Techniques

The joint inversion of passive seismic array data and H/V curves in order to obtain the V_S profile has been successfully used by a number of authors (Arai and Tokimatsu, 2005; Parolai *et al.*, 2005). The proposed procedure is not a joint H/V-array approach: it is single station H/V approach only, which does not require ancillary array measurements but requires some stratigraphic information. The use of array techniques in the present work is simply meant to validate the single station procedure.

Instrumentation

All single station tremor measurements in this work were performed with Tromino tromograph (Micromed SpA), a very compact (1 kg in weight), three-component, high sensitivity, and resolution (2200 V/m/sec, 24 dB, 0.1–250 Hz) tremor recorder.

When a sufficient number of instruments (mostly borrowed) became available, the ESAC and ReMi surveys were performed through synthetic aperture (global positioning system synchronized) 2D arrays of Trominos using up to nine elements with prime number monotonically increasing inter-instrument spacing. Tromino arrays were preferred, because they also allowed us to simultaneously record the H/V curves at each single point along the array. This, in turn, allowed us to interpret the variation in the H/V curves along the array as the effect of differences linked to subsoil stratigraphy under the sites of measure, because the difference in source/radiation could be excluded.

When a sufficient number of Trominos to deploy 2D arrays was not available, a SoilSpy Rosina (Micromed SpA) multichannel seismic digital acquisition system was used. The latter is a wired array with 16 vertical 4.5 Hz geophones; this wired array guarantees a signal to noise ratio that is superior to the traditional arrays, in which the analog signal is digitized only at the end of a $\simeq 10^2$ m long cable. Indeed, thanks to the larger number of sensors, this array provided clearer dispersion curves (see Sites I and IV in the Results

section) than Tromino arrays but lacked the advantage of simultaneous H/V acquisition at different points. However, in these cases we also used a lesser number of Trominos to simultaneously record H/V curves at some points along the array.

Results

We analyze results from selected sites in northern Italy that represent a variety of geological conditions. The location of the sites is shown in Figure 4, and for each site we show (Figs. 5–6 and 8–11) in panel (a) the array geometry; in panel (b) the H/V curves recorded at the same time along the array nodes, which allows us to check the 1D assumption for stratigraphy; in panel (c) the experimental H/V curve chosen as a representative for the site, the H/V marker corresponding to the known stratigraphic horizon, used to constrain the inversion (black arrow) and the fitted synthetic H/V curve (dark gray); in panel (d) the comparison (first validation step) between the theoretical Rayleigh-wave phase dispersion curve calculated for the model derived from the H/V fit (dark gray curve) together with the experimental dispersion curves derived from ESAC (light gray circles) and ReMi (contour plot) array surveys. The middle gray line is the best-fit dispersion curve obtained from a maximum likelihood inversion procedure for the arrays; in panel (e) the V_S profiles and V_{S30} values (second and third validation steps) obtained independently for the H/V and the array fit.

Site I

This site is located along the glacial deposit rim of the southern Alps. The underground structure has a 4 m thick soft silt layer, overlaying about 15 m of fluvio-glacial gravelly deposits in a fine-grain matrix, overlying in turn the bedrock. These two stratigraphic discontinuities (i.e., the related resonances of the above layers) have a signature in the H/V curve, which are the peaks at 10 and at 5 Hz, respectively (Fig. 5b). The H/V curves recorded along the long leg of the array deployed at this site (Fig. 5a) are all very similar; therefore, we had no problem in selecting an H/V curve representative of the site (square in Fig. 5a). We used the stratigraphic horizon at 4 m depth (resonance of the silt over the gravel), which is responsible for the H/V peak at 10 Hz (black arrow in Fig. 5c), to constrain the H/V inversion. This provides a starting value of $V_S \simeq 160$ m/sec for the first layer, according to equation (1), which is iteratively refined in the fitting process.

The first validation is illustrated in Figure 5d. Keeping in mind that according to the ReMi procedure, the picking of the dispersion curve should be performed on the lower margin of the maximum energy band, in order to accommodate for apparent rather than true velocities, we observe a good match of the different curves. This results in a very close match between the V_S profiles (Fig. 5e) that appear capable to recognize the two main stratigraphic discontinuities of the site and provide almost identical V_S values (second validation step) and V_{S30} within 5% (third validation step). Note that we needed only three layers to fit the H/V curve while we used six (which is the number fixed to fit all of the array dispersion curves in this study) for the array dispersion curves.

Figure 5e also shows the comparison between the model obtained from the H/V inversion and the stratigraphy. The V_S profile correlates well with the local geology.

Site II

This site is located in the river Po Plain, northeast of Italy. The underground structure has a first (5 m) layer of silts overlaying a large palaeochannel constituted of cemented sands. Below this palaeochannel, stiff clays are present. The knowledge of the underground structure comes from a number of penetration tests (up to 8 m depths) and a nearby 28 m deep drilling depth. Because the site is located in a large paleaochannel, we expect the 2D wave propagation effects to be small.

The H/V curves recorded at different nodes of the arrays deployed for the validation test (Fig. 6a) are practically identical (Fig. 6b), implying that the 1D assumption is valid. The experimental H/V curve selected for the fit (the square in Fig. 6a, but in this case any site along the array would give the same result), and the synthetic H/V curve are shown in Figure 6c. The stratigraphic horizon used to constrain the H/V fit is the contact between the shallow silts and the cemented palaeochannel located at 5 m depth, which corresponds to a strong increase in the N_{SPT} and is responsible for the H/V peak at 10 Hz (black arrow in Fig. 6c). According to equation (1), this provides a starting value $V_S \simeq 200$ m/sec for the first layer, which is iteratively refined in the fitting process.

The first validation step is illustrated in Figure 6d. The visual observation shows a good match of the various dispersion curves. It should be observed that at this site the array

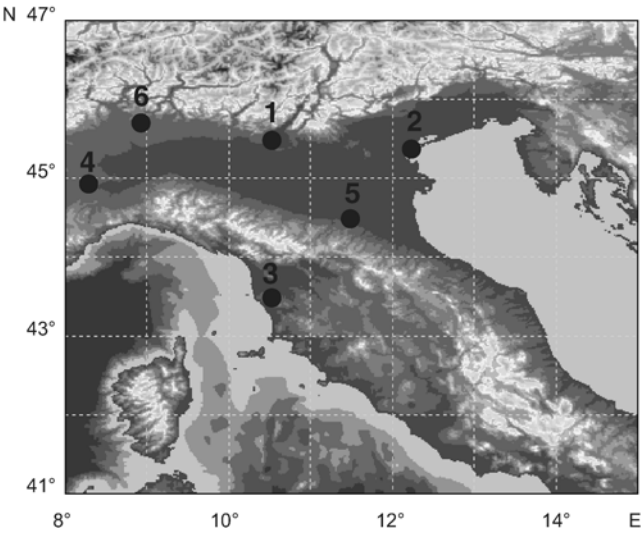

Figure 4. Location of the test sites in northern Italy.

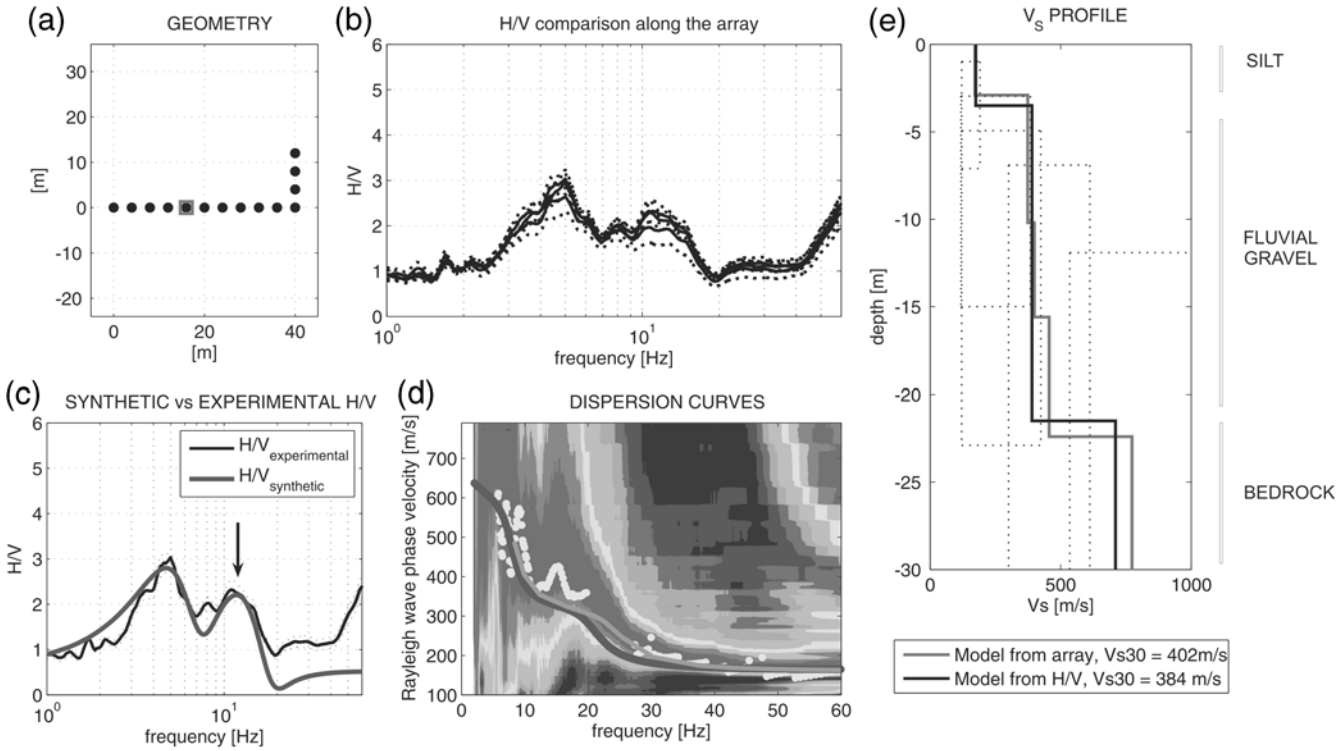

Figure 5. Site I. (a) H/V location and array geometry. (b) Comparison of the H/V recorded at different nodes of the array. Solid lines are the average H/V; dashed lines are the 2σ intervals. (c) Synthetic (light gray line) versus experimental (black line) H/V. Dotted lines are the 2σ intervals of the experimental H/V. (d) Dispersion curves from H/V fit (dark gray circles) and array inversion (light gray circles for 2D ESAC, contour map for 1D ReMi, and middle gray line for the best-fit model of ESAC and ReMi). (e) V_S profile inferred from H/V (black line) and array (light gray line) and geological model. The dotted boxes are the parameter spaces explored by the inversion routine for each layer.

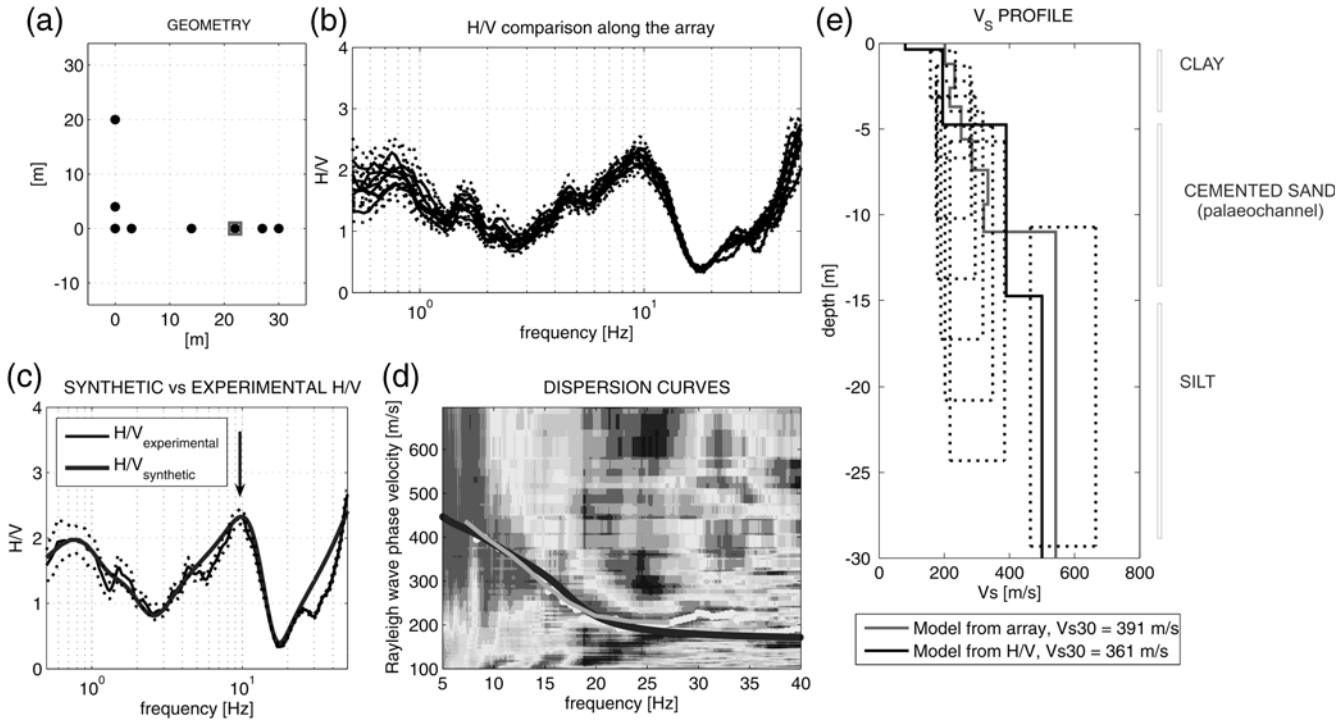

Figure 6. As in Figure 5 for Site II.

exploration does not give information below 9 Hz, corresponding to an explored wavelength of about 44 m, while the H/V does.

In the second validation step, the V_S profiles obtained from the H/V inversion and from the automatic inversion of the dispersion curves with four and eight layers, respectively, are compared in Figure 6e.

In the third validation step, the V_{S30} value provided by the H/V inversion is 361 m/sec, while the V_{S30} value provided by the automatic inversion of the dispersion curve gives 391 m/sec. The difference between our V_{S30} estimate and that of the array techniques is within 8%.

Figure 6e also shows the comparison between the model obtained from the H/V inversion and the stratigraphy. The V_S profile correlates well with the local geology.

Site III

This site is located on a harbor in central Italy. The array of Trominos was deployed on the stiff artificial soil (asphalt and compacted gravel) of the harbor barring the two ends that were directly set on the soft clay filled area.

This example is important in establishing the effect of a velocity inversion on the H/V. An extensive treatment of this effect can be found in Castellaro and Mulargia (2008). It is generally easy to distinguish the recordings taken on natural soil from those taken on stiff artificial soil, because recordings performed on layers more rigid than the underlying soils show a depression in the horizontal spectral component that shifts the H/V ratio to an amplitude lower than 1 for a wide frequency interval. The size of the H/V depression is a function of the stiff layer width, thickness, and rigidity in respect to the subsoil. This is clear in Figure 7c, where we plotted one of the curves recorded on natural soil (thin line) and one on the asphalt (thick line). Only the first one shows a $H/V > 1$ 10 Hz peak while the other curve results in H/V ratio <1 for the whole mid- to high-frequency range (3–60 Hz). The reversal in the normal spectral pattern above 3 Hz (i.e., horizontal components below the vertical component, $H/V < 1$) can be observed in Figure 7f and compared to Figure 7e. It should also be observed that the vertical spectral component is marginally affected in shape and still shows a local minimum pattern (black arrow in panel [f]) that is the relic of the resonance peak at 10 Hz. A synthetic modeling of the H/V resulting on natural soil and on asphalt is given in Figure 7d for the stratigraphy shown in panels (a) and (b), which differs only for the first 20 cm of stiffer soil.

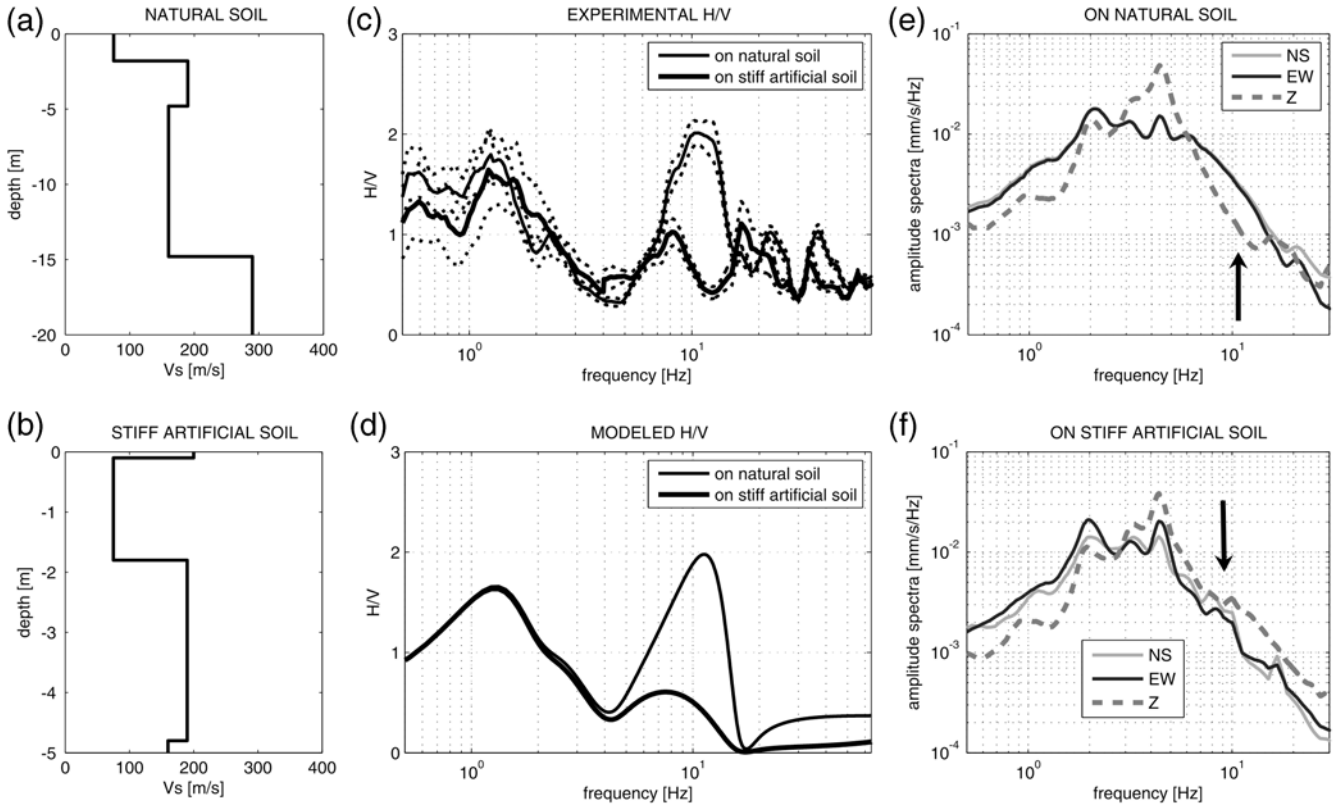

Figure 7. Site III. Effect of a velocity inversion induced by a stiff artificial layer on H/V. (a) Stratigraphic model on natural soil. (b) Stratigraphic model on stiff artificial soil (zoom on the first 5 m only, for $z < -5$ m model as in panel [a]). (c) Experimental H/V curves on natural (thin lines) and on stiff artificial (thick lines) soil. (d) Modeled H/V for the case on natural soil of panel (a) (thin line) and on the stiff artificial soil of panel (b) (thick line). (e) Typical spectra on natural soil. (f) Typical spectra on stiff artificial soil. The arrow indicates the eye-shaped spectral pattern responsible for the H/V peak on natural soil (panel [e]) and the same pattern on stiff artificial soil (panel [f]) which, due to the depression of the horizontal spectral components, cannot result in an H/V larger than 1.

The synthetic H/V curves of panel (d) match the experimental curves of panel (c) very well.

At this site, we know that there is an anthropogenic accumulation of very soft detrital clays for 2 m, above the on-site natural clays. To constrain the H/V fit, we selected the H/V curve at one end of the array (square in Fig. 8a), where the high-frequency (11 Hz) peak related to this stratigraphic horizon can be clearly seen (black arrow in Fig. 8c). This provides a starting value of $V_S \simeq 90$ m/sec for the first layer, according to equation (1), which is iteratively refined in the fitting process.

The first validation is illustrated in Figure 8d and shows a good match of the different curves, which results in a good match between the V_S profiles (Fig. 8e) and a V_{S30} value within 2%.

Site IV

At this site (plane region in the northwest part of Italy), the direct prospection shows the presence of silts and the top of a rigid gravel layer at 10 m depth. The marker of this clear stratigraphic horizon is interpreted as the H/V peak at 5 Hz (Fig. 9b), which suggests for the silt layer a $V_S \simeq 200$ m/sec that is iteratively refined in the fitting process. The array and H/V measurements were set on an artificially stabilized soil; this explains the moderate shallow velocity inversion suggested by the H/V, which is persistently < 1 for frequencies above 7 Hz. One should keep in mind that velocity inversions lower the H/V amplitude down to the first resonance peak included (Castellaro and Mulargia, 2008). This implies that the velocity inversion must be comprehended in the subsoil model in order to adequately fit the experimental H/V curve.

The H/V profile along the section reveals a substantially 1D subsoil. The correspondence between the dispersion curves appears satisfactory (Fig. 9d) and the V_{S30} values provided by the single station and array techniques are within 12%.

Site V

This case is relative to a site in the river Po Plain, where only fine-grained sediments are present. The peculiarity of this example is the shallow velocity inversion due to the presence of the uppermost 4 m of overconsolidated clay overlying softer clays, which sets the H/V amplitude below 1 from about 15 Hz downwards (Castellaro and Mulargia, 2008).

The H/V curves acquired at different points, later used as array nodes (Fig. 10a), show practically no variability (Fig. 10b). The stratigraphy was known from five penetration tests reaching depths from 10 to 17 m.

We constrained the inversion to the depth of the velocity inversion (4 m, about 15 Hz at the selected point, Fig. 10c). According to equation (1), this provides for the first layer, a first iteration $V_S \simeq 150$ m/sec.

The first validation step is illustrated in Figure 10d: the dispersion curves from the H/V fit and, from the array methods, agree well. As a consequence, the second validation step, that is, the comparison between V_S profiles, also shows a satisfying agreement between the single station and the ar-

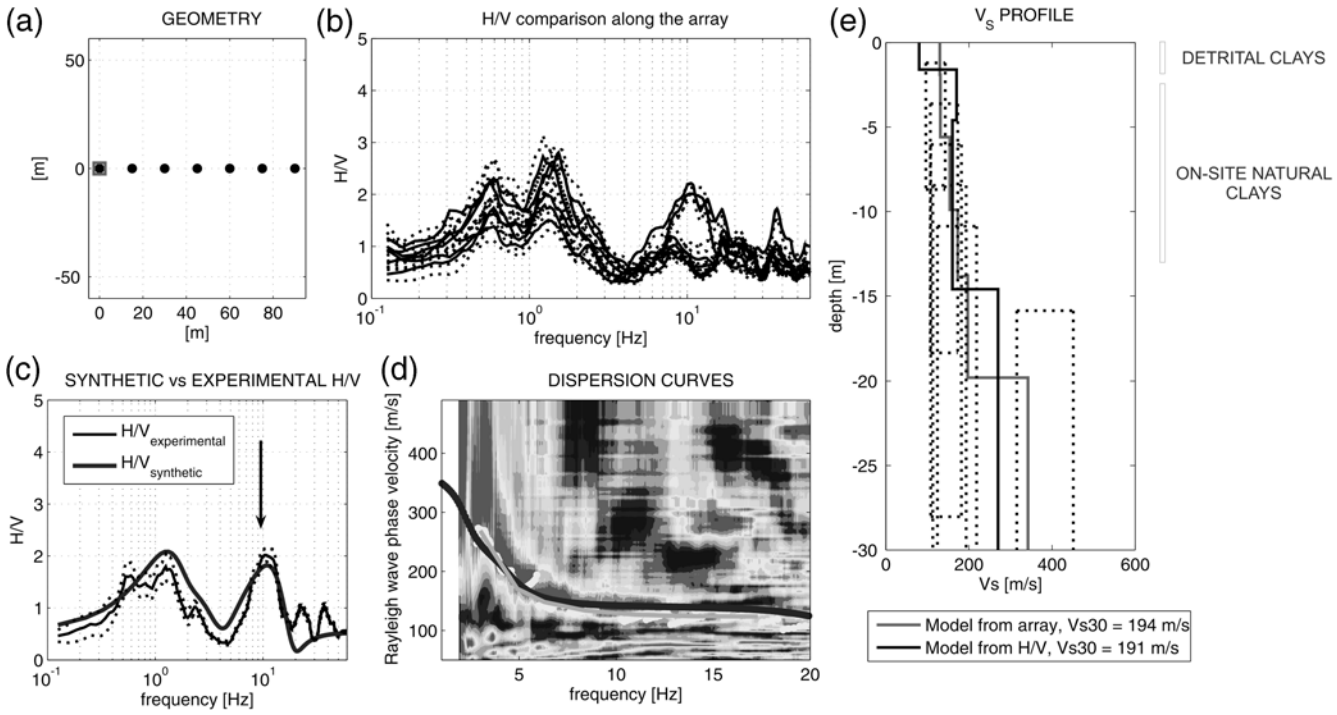

Figure 8. As in Figure 5 for Site III.

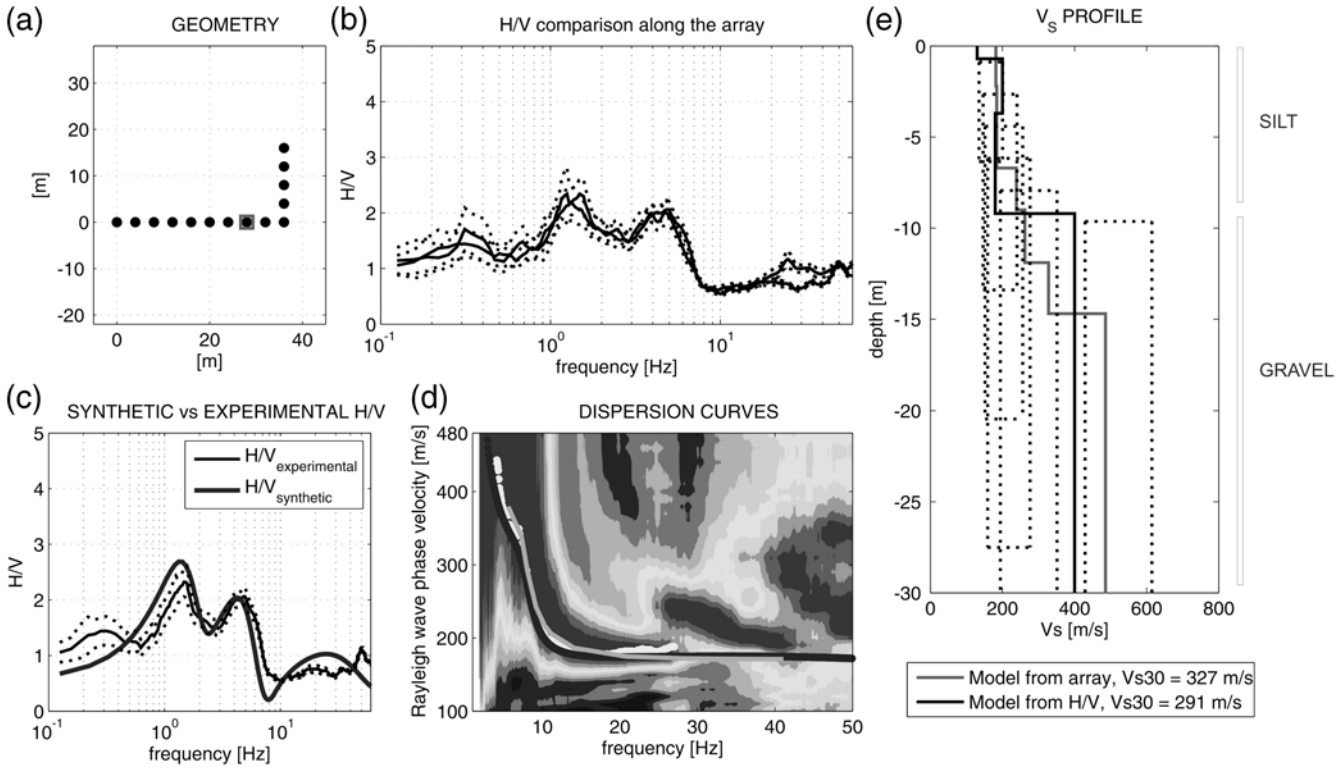

Figure 9. As in Figure 5 for Site IV.

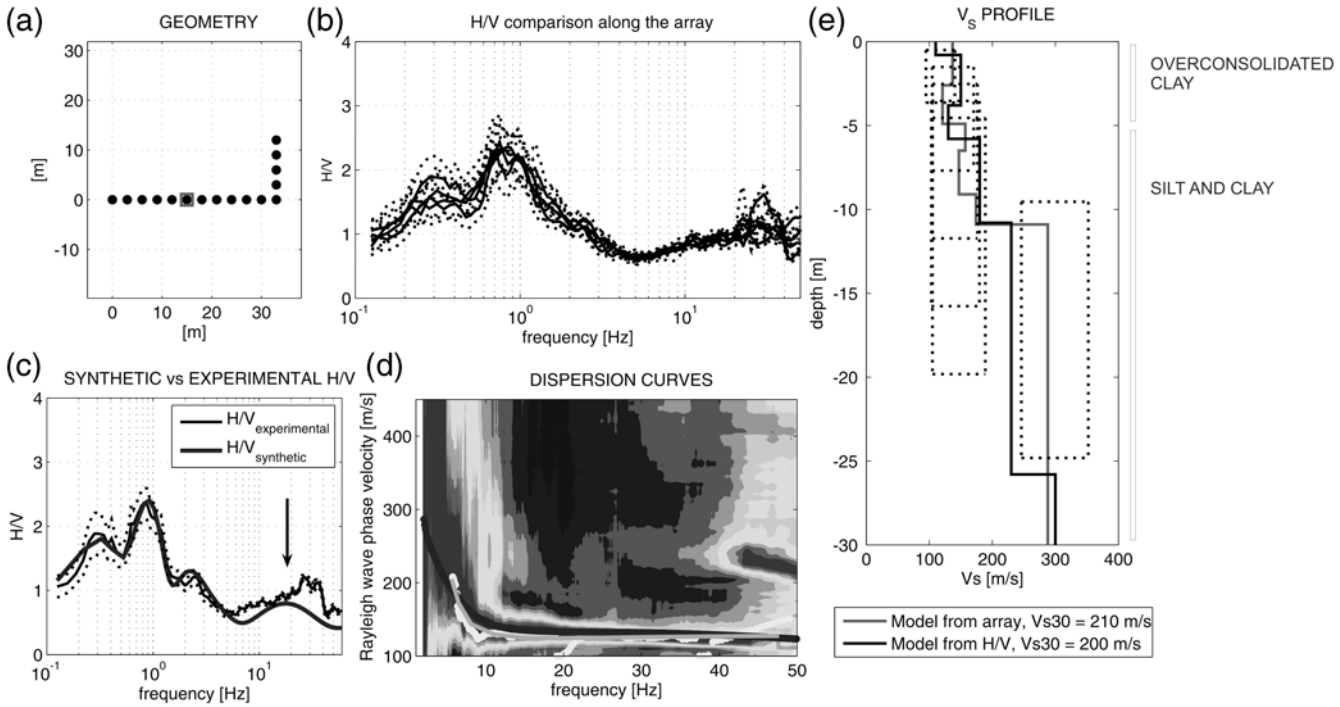

Figure 10. As in Figure 5 for Site V.

ray technique. The V_{S30} values (third validation step) are within 5%.

Site VI

As a last case, we show an example from the northwest part of Italy. It is relative to a plane area that experienced glacial events in the past and therefore has a very complex geology, modeled by turbulent glacial rivers and deposits. It is impossible to define a common stratigraphic setting for this area because the picture continuously changes even at sites 3 m apart, as shown by the dozen of drillings, penetration tests, and refraction surveys in the very small investigated area.

The H/V curves recorded at the nodes of the arrays used for the validation test (Fig. 11a) confirm very large variations (Fig. 11b), implying that the 1D assumption definitely does not hold even at a distance of 30 m in this case .

Because a typical H/V curve cannot be defined along the array, we simply selected one of them (the square in Fig. 11a) for the inversion (Fig. 11c) and constrained it to the horizon at a 9 m depth (7 Hz) that was found by the drilling at that site. This provides a first iteration of $V_S \simeq 250$ m/sec for the first layer, according to equation (1).

In the first validation step, the dispersion curve resulting from the model used to fit the experimental H/V is superimposed to the dispersion curve resulting from ESAC and the contour map resulting from ReMi (Fig. 11d). As can reasonably be expected, the dispersion curves do not match below 15 Hz.

In the second and third validation steps, we compare the V_S profile and V_{S30} values provided by the H/V fit and those provided by the automatic inversion of the dispersion curves from the array investigation (Fig. 11e). Note how V_{S30} are still within a 20% difference, which looks acceptable if it is compared to the very peculiar conditions of this case, in which all estimates must be regarded as very approximate.

Discussion and Conclusion

Seismic codes in most countries require an estimate of the V_{S30} parameter for microzonation not only at the regional scale but also at the scale of the single building. In this article, we propose a procedure to estimate the V_{S30} parameter based on a constrained fit of single station H/V curves. The proposed technique requires the knowledge of the depth of a stratigraphic horizon, which is usually available in geotechnical practice that can be linked to a feature in the H/V curve. Under increasing V_S profiles with depth, this feature is usually an H/V peak. Under velocity inversions, the H/V curve is lowered below 1 for a wide frequency range (Castellaro and Mulargia, 2008); a joint interpretation of H/V and single component spectra is required. As a consequence, H/V measurements on artificial soils stiffer than subsoil should always be avoided.

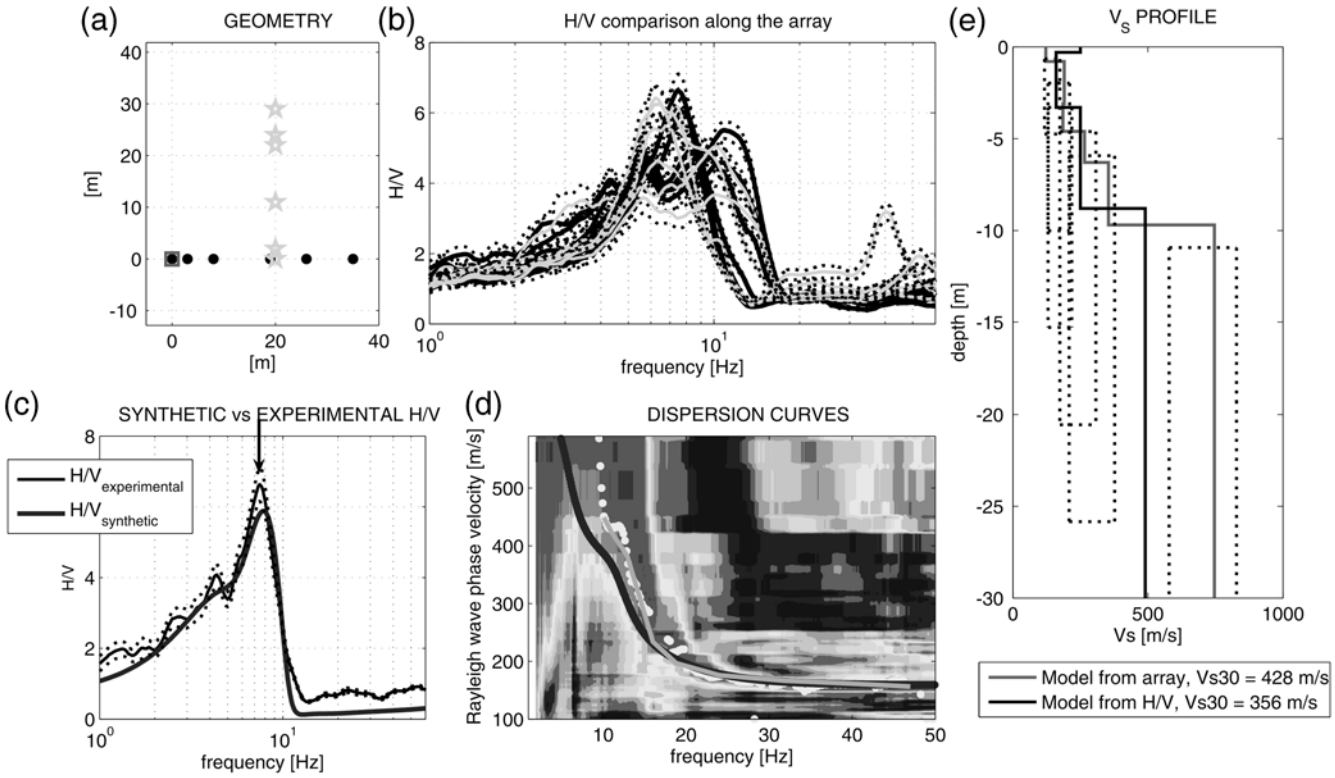

Figure 11. As in Figure 5 for Site VI.

The cases presented in this study cover a variety of geological conditions and show that the technique has the potential to provide V_{S30} estimates that are coherent with those provided at the same sites by ESAC and ReMi array techniques and are adequate to comply with the seismic codes. Obviously, the H/V single station measurements have the additional bonus of providing a measure of the main resonance frequency of the sedimentary layer.

As with any technique, the proposed procedure relies on a number of assumptions. Among these, a crucial one is the 1D subsoil model. Simultaneous H/V measurements at distances of a few (less than five) meters, even in plane areas, often showed differences that appear incompatible with 1D subsurface geometry. This should be considered when comparing results obtained from array techniques, which often span more than 100 m, with those from H/V fit.

A second limitation is that microtremor composition is still debated and all fitting procedures could be questionable to some extent.

Because the H/V amplitude at low frequency (below 0.8–0.5 Hz) is weather dependent (Mulargia and Castellaro, 2007), the H/V fit technique adopted in this study is only aimed at shallow subsoil analysis and should not be considered applicable below 0.8–0.5 Hz.

The proposed technique is therefore not aimed to provide precise V_S profiles but appears to give estimates of the V_{S30} parameter that are adequate enough to satisfy law requirements.

Data and Resources

All of the data showed in this study were recorded by the authors with Tromino and SoilSpy Rosina (Micromed spa) instruments and were analyzed with software that they also developed. All of the data are proprietary to the authors.

Acknowledgments

S. C. is indebted to Francesco Baliva for useful discussions on array processing. F. M. thanks Giuliano Francesco Panza for enlightening discussions on modal summation in laterally heterogeneous media. The authors are also grateful to the professional geologists who gave them access to data from penetration tests and/or drillings, in particular, Dario Battistella, Nicola Negri, and Loredana Zecchini.

Reference

Arai, H., and K. Tokimatsu (2005). *S*-wave velocity profiling by joint inversion of microtremor dispersion curve and horizontal-to-vertical (H/V) spectrum, *Bull. Seismol. Soc. Am.* **95,** 1766–1778.

Ben-Menahem, A., and S. J. Singh (1981). *Seismic Waves and Sources*, Springer-Verlag, New York, 1108 pp.

Bodin, P., K. Smith, S. Horton, and H. Hwang (2001). Microtremor observations of deep sediment resonance in metropolitan Memphis, Tennessee, *Eng. Geol.* **2,** 159–168.

Bonnefoy-Claudet, S., A. Köhler, C. Cornou, M. Wathelet, and P.-Y. Bard (2008). Effects of Love waves on microtremor H/V ratio, *Bull. Seismol. Soc. Am.* **98,** 288–300.

Campillo, M., and A. Paul (2003). Long range correlations in the diffuse seismic coda, *Science* **299,** 547–549.

Castellaro, S., and F. Mulargia (2009). The effect of velocity inversions on H/V, *Pure Appl. Geophys.* (accepted).

Castellaro, S., F. Mulargia, and L. Bianconi (2005). Passive seismic stratigraphy: a new efficient, fast and economic technique, *J. Geotech. Environ. Geol.* **3,** 51–77.

Castellaro, S., F. Mulargia, and P. M. Rossi (2008). V_{S30}: proxy for seismic amplification?, *Seism. Res. Lett.* **79,** 540–542.

Del Pezzo, E., S. De Martino, F. De Miguel, J. Ibanez, and A. Sorgente (1991). Characteristics of the seismic attenuation in two tectonically active zones of southern Europe, *Pure Appl. Geophys.* **135,** 91–106.

Dunkin, J. W. (1965). Computation of modal solutions in layered, elastic media at high frequencies, *Bull. Seismol. Soc. Am.* **55,** 335–358.

Fäh, D., F. Kind, and D. Giardini (2001). A theoretical investigation of average H/V ratios, *Geophys. J. Int.* **145,** 535–549.

Guéguen, P., J.-L. Chatelain, B. Guillier, H. Yepes, and J. Egred (1998). Site effect and damage distribution in Pujili (Ecuador) after the 28 March 1996 earthquake, *Soil. Dyn. Earthq. Eng.* **17,** 329–334.

Guillier, B., J. L. Chatelain, M. Hellel, D. Machane, N. Mezouer, R. Ben Salem, and E. H. Oubaiche (2005). Smooth bumps in H/V curves over a broad area from single-station ambient noise recordings are meaningful and reveal the importance of Q in array processing: the Boumerdes (Algeria) case, *Geophys. Res. Lett.* **32,** L24306, doi 10.1029/2005GL023726.

Ibs-von Seht, M., and J. Wohlenberg (1999). Microtremor measurements used to map thickness of soft sediments, *Bull. Seismol. Soc. Am.* **89,** 250–259.

Jeng, Y., J.-Y. Tsai, and S.-H. Chen (1999). An improved method of determining near-surface Q, *Geophysics* **64,** 1608–1617.

Köhler, A., M. Ohrnberger, F. Scherbaum, M. Wathelet, and C. Cornou (2007). Assessing the reliability of the modified three-component spatial autocorrelation technique, *Geophys. J. Int.* **168,** 779–796, doi 10.1111/j.1365-246X.2006.03253.x.

Lachet, C., and P.-Y. Bard (1994). Numerical and theoretical investigations on the possibilities and limitation of Nakamuras technique, *J. Phys. Earth* **42,** 377–397.

Lermo, J., and F. J. Chavez-Garcia (1993). Site effect evaluation using spectral ratios with only one station, *Bull. Seismol. Soc. Am.* **83,** 1574–1594.

Lermo, J., and F. J. Chavez-Garcia (1994). Are microtremors useful in site response evaluation?, *Bull. Seismol. Soc. Am.* **84,** 1350–1364.

Louie, J. (2001). Faster, better: shear-wave velocity to 100 meters depth from refraction microtremor arrays, *Bull. Seismol. Soc. Am.* **91,** 347–364.

Malagnini, L. (1996). Velocity and attenuation structure of very shallow soils: evidence for a frequency-dependent Q, *Bull. Seismol. Soc. Am.* **86,** 1471–1486.

Malin, P. E., J. A. Waller, R. D. Borcherdt, E. Cranswick, E. G. Jensen, and J. Van Schaack (1988). Vertical seismic profiling of Oroville microearthquakes: velocity spectra and particle motion as a function of depth, *Bull. Seismol. Soc. Am.* **78,** 401–420.

Marquardt, D. W. (1963). An algorithm for least-squares estimation of nonlinear parameters, *J. Soc. Ind. Appl. Math.* **11,** 431–441.

Mulargia, F., and S. Castellaro (2007). Single-station passive seismic stratigraphy to nearly 2 km depth in sedimentary basins, in the *Proc. of the International Union of Geodesy and Geophysics XXIV General Assembly*, Perugia, Italy2-13 July 2007.

Mulargia, F., and S. Castellaro (2008). Passive imaging in nondiffuse acoustic wavefields, *Phys. Rev. Lett.* **100,** 218501(1–4).

Müller, T. M., and S. A. Shapiro (2001). Seismic scattering attenuation estimates for the German KTB area derived from well-log statistics, *Geophys. Res. Lett.* **28,** 3761–3764.

Ohori, M., A. Nobata, and K. Wakamatsu (2002). A comparison of ESAC and FK methods of estimating phase velocity using arbitrarily shaped microtremor arrays, *Bull. Seismol. Soc. Am.* **92,** 2323–2332.

Parolai, S., G. Grünthal, and R. Wahlström (2007). Site-specific response spectra from the combination of microzonation with probabilistic seis-

mic hazard assessment—an example for the Cologne (Germany) area, *Soil Dyn. Earthq. Eng.* **27,** 49–59.

Parolai, S., M. Picozzi, S. M. Richwalski, and C. Milkereit (2005). Joint inversion of phase velocity dispersion and H/V curves from seismic noise recordings using a genetic algorithm, considering higher modes, *Geophys. Res. Lett.* **32,** L01301, doi 10.1029/2004GL021115.

Romanowicz, B. (2003). *International Handbook of Earthquake and Engineering Seismology*, W. H. K. Lee, H. Kanamori, P. C. Jennings and C. Kisslinger (Editors), Academic, New York.

Roux, P., W. A. Kuperman, and the NPAL Group (2004). Extracting coherent wave fronts from acoustic ambient noise in the ocean, *J. Am. Acoust. Soc.* **116,** 1995–2003.

Sax, R. L., and R. A. Hartenberger (1964). Theoretical prediction of seismic noise in a deep borehole, *Geophysics* **29,** 714–720.

Site EffectS assessment using AMbient Excitations (2005). http:sesame-fp5 .obs.ujf-grenoble.fr, last accessed 22 December 2008.

Shapiro, N. M., and M. Campillo. (2004). Emergence of broad band Rayleigh waves from correlations of the ambient seismic noise, *Geophys. Res. Lett.* **31,** L07614, doi 10.1029/2004GL019491.

Tanimoto, T. (1987). The three-dimensional shear wave structure in the mantle by overtone waveform inversion. I. radial seismogram inversion, *Geophys. J. R. Astr. Soc.* **89,** 713–740.

Dipartimento di Fisica
Settore di Geofisica
Università di Bologna
Viale Carlo Berti Pichat 8
40127 Bologna, Italy
silvia.castellaro@unibo.it
francesco.mulargia@unibo.it

Manuscript received 1 August 2007